



# High-power two-cycle ultrafast source based on hybrid nonlinear compression

L. Lavenu, M. Natile, F. Guichard, Xavier Délen, Marc Hanna, Y. Zaouter,  
Patrick Georges

## ► To cite this version:

L. Lavenu, M. Natile, F. Guichard, Xavier Délen, Marc Hanna, et al.. High-power two-cycle ultrafast source based on hybrid nonlinear compression. *Optics Express*, 2019, 27 (3), pp.1958-1967. 10.1364/OE.27.001958 . hal-02106501

**HAL Id: hal-02106501**

**<https://hal-iogs.archives-ouvertes.fr/hal-02106501>**

Submitted on 23 Apr 2019

**HAL** is a multi-disciplinary open access archive for the deposit and dissemination of scientific research documents, whether they are published or not. The documents may come from teaching and research institutions in France or abroad, or from public or private research centers.

L'archive ouverte pluridisciplinaire **HAL**, est destinée au dépôt et à la diffusion de documents scientifiques de niveau recherche, publiés ou non, émanant des établissements d'enseignement et de recherche français ou étrangers, des laboratoires publics ou privés.



# High-power two-cycle ultrafast source based on hybrid nonlinear compression

L. LAVENU,<sup>1,2</sup> M. NATILE,<sup>2,3</sup> F. GUICHARD,<sup>2</sup> X. DÉLEN,<sup>1</sup> M. HANNA,<sup>1,\*</sup> Y. ZAOUTER,<sup>2</sup> AND P. GEORGES<sup>1</sup>

<sup>1</sup>Laboratoire Charles Fabry, Institut d'Optique Graduate School, CNRS, Université Paris-Saclay 91127, Palaiseau Cedex, France

<sup>2</sup>Amplitude Laser Group 33600, Pessac, France

<sup>3</sup>LIDyL, CEA, CNRS, Université Paris-Saclay, CEA-SACLAY 91191, Gif-sur-Yvette, France

\*marc.hanna@institutoptique.fr

**Abstract:** We demonstrate a hybrid dual-stage nonlinear compression scheme, which allows the temporal compression of 330 fs-pulses down to 6.8 fs-pulses, with an overall transmission of 61%. This high transmission is obtained by using a first compression stage based on a gas-filled multipass cell, and a second stage based on a large-core gas-filled capillary. The source output is fully characterized in terms of spectral, temporal, spatial, and short- and long-term stability properties. The system's compactness, stability, and high average power makes it ideally suited to drive high photon flux XUV sources through high harmonic generation.

© 2019 Optical Society of America under the terms of the [OSA Open Access Publishing Agreement](#)

## 1. Introduction

Few-cycle laser sources are the subject of intense research efforts worldwide since they allow efficient high-harmonic generation (HHG) and the emission of isolated attosecond pulses. This results in compact and highly coherent radiation sources in the extreme ultraviolet (XUV) and soft X-ray ranges, with a rapidly increasing number of scientific and industrial applications such as ultrafast spectroscopy, nanoscale imaging, and attosecond science [1–3]. Laser sources based on titanium-doped sapphire (Ti:Sa) have, for a long time, been almost exclusively used to drive the HHG process and to pioneer attosecond physics. The pulse duration typically available from such lasers is 25 fs, so that a single stage of nonlinear compression in a gas-filled capillary result in few-cycle pulses [4]. Despite extraordinary material properties such as gain bandwidth and thermal conductivity, Ti:Sa systems suffer from the short upper state lifetime, their large quantum defect and the fact that they must be pumped with high brightness green lasers. This limits the efficiency, output average power, and prevents repetition rate scaling to drive strong field physics experiments.

Laser physicists have been working on more efficient and power scalable ultrafast sources for strong field physics for over a decade. In particular, optical parametric chirped pulse amplifier systems appear as a particularly promising solution [5,6], since they can deliver extremely short pulses in various wavelength ranges and are less impacted by thermal effects because they are based on a non-resonant nonlinear process. However, in order to obtain good spatial and temporal quality, the energy transfer from the pump to the signal is around 10%, so that the pump laser energy must be scaled accordingly, with stringent requirements in terms of spatial and temporal quality.

Currently, the most mature and powerful ultrafast source technology is undoubtedly ytterbium-based systems, with average power levels beyond 1 kW [7–9] and numerous industrial applications. These lasers have been used to drive the HHG process as early as 2009 [10], but the long pulse duration delivered by these sources (300 fs – 2 ps) limits their relevance to this application field. Therefore, nonlinear compression setups have been used successfully to reduce the pulse duration and obtain XUV photon flux among the highest ever reported for HHG-based sources [11]. However, to reach sub-3 cycles regime (< 10 fs at 1030

nm), which is typically required in combination with gating techniques to obtain isolated attosecond pulses, two stages of compression must usually be implemented [12]. This reduces the energy efficiency of Yb-based systems dedicated to attosecond physics.

In this article, we describe a two-stage nonlinear compression setup that provides enough compression ratio to reach sub-10 fs pulse duration from a high-energy ytterbium-doped fiber amplifier (YDFA) laser, while ensuring the highest transmission (61%) ever reported for two cascaded stages. This results in the generation of 6.8 fs, 140  $\mu$ J pulses at 150 kHz repetition rate, corresponding to 21 W average power. These performances are achieved by combining two nonlinear compression technologies, first a gas-filled multipass cell, and second a large diameter-core capillary. The described laser system is robust, compact, and power efficient, making it an ideal driver laser for application-ready high flux XUV and attosecond sources.

## 2. Rationale

Gas-filled capillaries are the most widespread nonlinear media used to temporally compress femtosecond pulses with energies above 100  $\mu$ J. Propagation in this lossy waveguide imparts spectral broadening through the self-phase modulation (SPM) effect along with a frequency chirp that can be removed by dispersive optics at the output of the capillary. The capillary diameter choice is bounded by two phenomena: it should be large enough to avoid significant ionization of the gas, and small enough to induce sufficient SPM, which directly translates to the compression ratio. The gas nature and pressure inside the capillary is limited by the threshold for self-focusing, which does not depend on the diameter. Moreover, for practical reasons and to ensure a reasonable footprint, the capillary length is often of the order of 1 m. As a consequence, for pulse durations of 300 fs and energies between 100  $\mu$ J and 1 mJ, as is standard at the output of YDFA systems, a capillary diameter of 250  $\mu$ m is often used to obtain a compression ratio around 10. In a laboratory environment where longer capillaries with larger diameters can be used, a recent experiment demonstrates a compression ratio of 33 in a 6-m-long 500- $\mu$ m-diameter capillary with a transmission of 70% [13].

On the other hand, the losses introduced by a capillary are related to two parameters: the spatial quality of the input laser, which determines the fraction of energy that can be coupled to the fundamental mode exhibiting the lowest losses, and the ratio of diameter to central wavelength, which determines the losses of each capillary mode. YDFA systems often exhibit close-to-perfect spatial quality, so that the losses are dominated by the capillary losses. Experimentally obtained transmission factors for such setups at the output of YDFA are in the range of 60% (single stage) to 30% (dual-stage) [12,14].

To increase this transmission, and allow energy scaling of compression setups, a recently demonstrated technique consists in propagating the pulses to be compressed in a multipass cell (MPC) that includes a nonlinear medium [15]. The MPC is formed by an arrangement of concave mirrors and the input beam is matched to the stationary beam in the cell. As it propagates through a large number of roundtrips, the input pulse is periodically focused. If the nonlinearity per roundtrip is kept sufficiently small, the spatial Kerr effect is redistributed over the whole beam, ensuring high spatial quality at the output, despite a possibly large accumulated temporal B-integral [16]. This technique can be considered as an extension of multi-plate setups [17–19] with a distribution of the nonlinearity over tens of passes in the material instead of few, inducing a better output spatial quality and allowing higher compression factors. Compared to capillaries, this technique provides several additional degrees of freedom in terms of geometry, nonlinear material used (solid [15,20] or gas [21,22]), and spectral phase control through the mirror coatings. The most obvious improvement is that, using commercially available mirrors, the transmission of the cell is above 90% in all reported demonstrations. One drawback of cell-based setups to reach very short pulse durations, however, is that the pulses undergo a large number of reflections on the cell mirrors (several tens), so that spectral phase aberrations induced by the mirrors are magnified. The design requirements on the mirrors in terms of bandwidth, spectral phase

control, reflectivity, and damage threshold, are more and more difficult to meet as the pulse duration decreases and the energy increases.

We therefore propose a hybrid two-stage compression setup design that first uses a gas-filled MPC to take advantage of its large transmission. This stage allows compressing the YDFA output to around 40 fs, corresponding to a compression ratio of 8, with an efficiency as high as 85%. The corresponding optical bandwidth is narrow enough to relax the constraint on the MPC mirror design. At the output of this first stage the peak power is increased compared to the laser output, allowing the use of a second stage based on a large core diameter capillary of 400  $\mu\text{m}$ , which increases the transmission of this second stage to 72%. The use of a capillary for the second stage also alleviates the problem of extreme bandwidth requirement for the MPC mirror. These two techniques are therefore perfectly complementary and allow access to the few-cycle regime from Yb-based lasers with a record efficiency of 61%.

### 3. Experimental setup

The experimental setup is sketched in Fig. 1 and fits in a footprint of  $1.8\text{ m} \times 1.0\text{ m}$ . It starts with an YDFA source that delivers 330 fs 225  $\mu\text{J}$  pulses at 150 kHz repetition rate, corresponding to an average power of 34 W. The  $M^2$  beam quality factor measured at the output of the laser is  $1.4 \times 1.2$ . The pulse temporal profile and spectrum, measured using a second-harmonic frequency resolved optical gating (FROG) apparatus, are shown in Fig. 2 along with the collimated beam spatial profile.

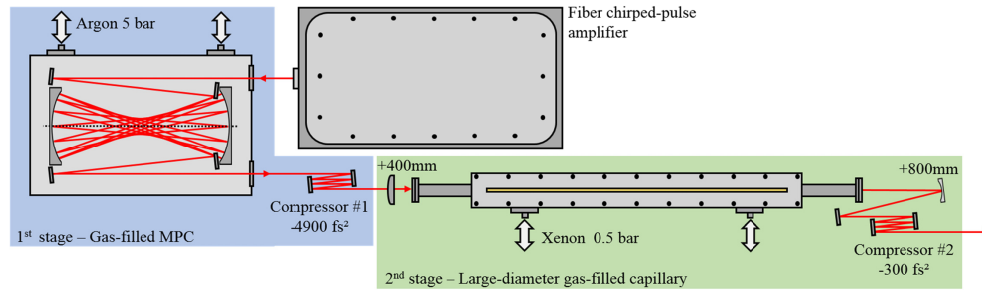


Fig. 1. Experimental setup of the hybrid, two-stage nonlinear compression source.

The beam is sent to the first stage of nonlinear compression based on a gas-filled MPC, which is similar to the one described in [21]. Mode-matching to the stationary MPC beam is achieved using an arrangement of lenses. The beam is coupled in and out of the cavity using small plane rectangular mirrors located in front of the cell mirrors. These are two identical low-group delay dispersion (GDD) mirrors with a diameter of 2 inches and a radius of curvature 300 mm, separated by 450 mm, inside a pressure chamber filled with 5 bar of argon. The stationary beam has a  $1/e^2$  radius of 206  $\mu\text{m}$  at the MPC waist, expanding to 412  $\mu\text{m}$  on the MPC mirrors. The in- and out-coupling mirrors are aligned for the beam to go through 27 roundtrips, corresponding to a total propagation length of 24.3 m inside the MPC. The nonlinear index of the gas at this pressure level is  $n_2 = 4.65 \times 10^{-23} \text{ m}^2/\text{W}$  [23], corresponding to a self-focusing threshold of 2.8 GW, well above the input peak power estimated to be 540 MW. At the output of the MPC, dispersive mirrors are inserted with a total GDD of  $-4900 \text{ fs}^2$ .

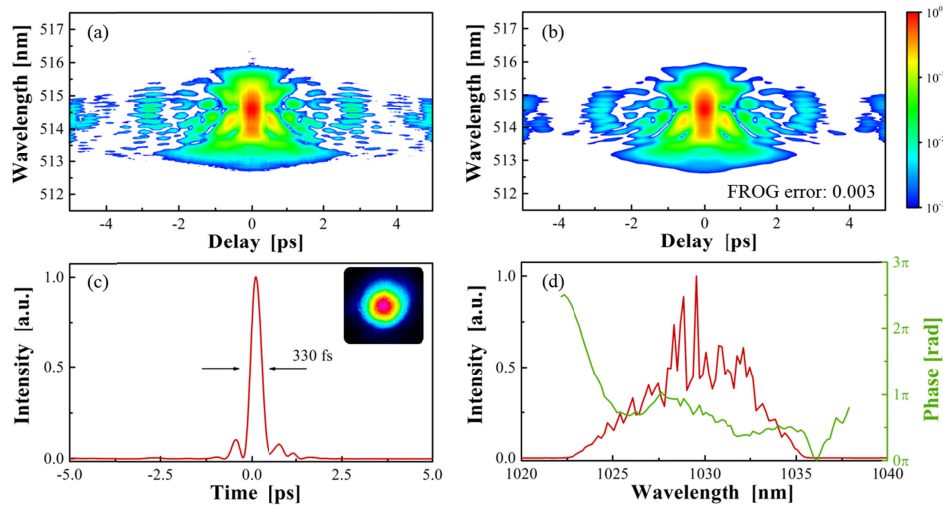


Fig. 2. Measured (a) and retrieved (b) FROG traces at the output of the YDFA. Temporal profile (c, far-field spatial profile in inset) and spectral intensity and phase (d).

The beam is then sent to the second nonlinear compression stage based on a 400  $\mu\text{m}$  diameter 1 m-long capillary filled with 500 mbar of Xenon. A  $f = 400$  mm lens is used to focus the beam at the input facet of the capillary. The corresponding nonlinear index and critical power are  $n_2 = 2.5 \times 10^{-23} \text{ m}^2/\text{W}$  [23] and 5.3 GW respectively, with an estimated peak power at the input of the capillary of 3.5 GW. The output beam is finally collimated and sent to a pair of chirped mirrors introducing a total GDD of  $-300 \text{ fs}^2$ . An additional pair of  $\text{CaF}_2$  wedges allows fine tuning the compression.

#### 4. First stage: multi-pass cell

Figure 3 shows the experimental results obtained at the output of the first MPC-based nonlinear compression stage, including a FROG characterization and collimated beam profile at the output. The spectrum is broadened, with a  $-10$  dB bandwidth of 65 nm, while the pulse is compressed to 43 fs. This moderate compression ratio allows excellent temporal quality, with a Fourier transform-limited (FTL) pulse duration of 40 fs, and a temporal Strehl ratio of 87%.

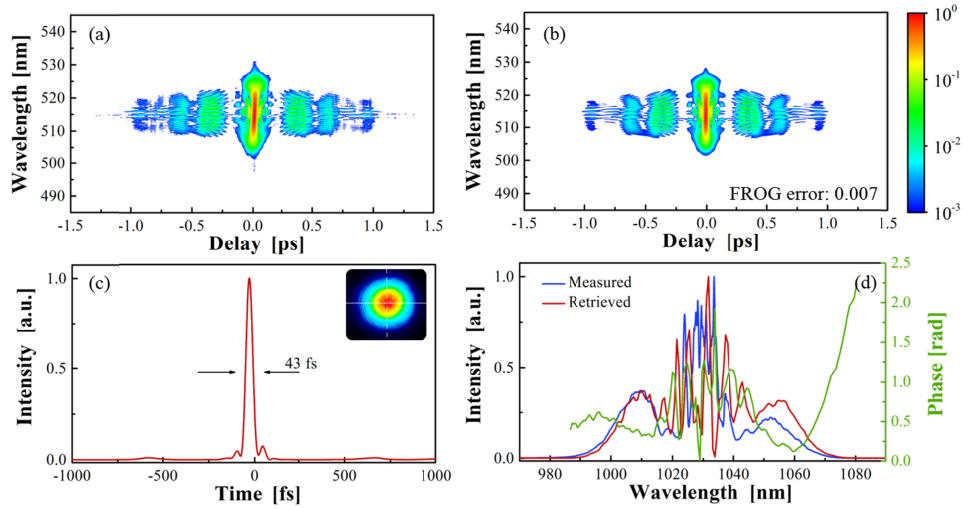


Fig. 3. Measured (a) and retrieved (b) FROG traces at the output of the MPC stage. Temporal profile (c) (far-field spatial profile in inset) and spectral intensity and phase (d).

The spatial quality at the output is also excellent, with measured  $M^2$  factors of  $1.2 \times 1.2$ . This slight improvement over the input beam quality is observed in a reproducible way, which deserves future detailed investigations. The total transmission of this compression stage, including mode-matching optics and dispersive mirrors, is 85%. The compressed pulse energy is therefore 190  $\mu$ J, corresponding to an average power of 28.7 W.

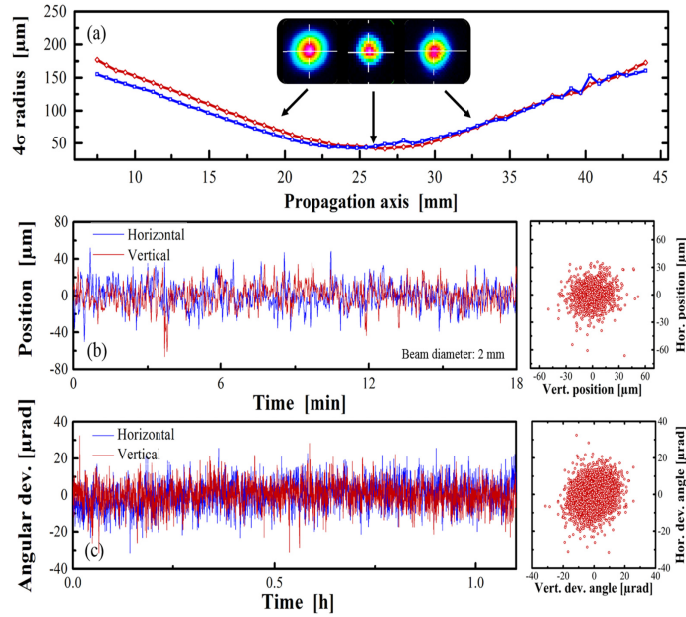


Fig. 4. Additional characterization at the output of the MPC. (a) Beam caustic measurement along two orthogonal axes. (b) Beam position stability measurement. (c) Beam pointing stability measurement.

At this intermediate stage, the stability properties are essential. Indeed, intensity or beam pointing instabilities could be exacerbated by the second capillary-based nonlinear



compression stage. We therefore thoroughly characterized these properties (with a special emphasis on relative intensity noise in section 6). As shown in Fig. 4, the RMS beam pointing stability over 1h is 13  $\mu\text{rad}$ , and the beam position stability is 24  $\mu\text{m}$  over 20 min, for a beam diameter of 2 mm at  $1/e^2$ . These excellent stability properties allow us to use it confidently as the input to the second capillary-based stage.

### 5. Second stage: large-diameter capillary

Figure 5 shows the temporal and spectral characterization at the output of the capillary stage, performed using a d-scan apparatus [24] (Sphere Photonics) designed for measurement of pulsewidths down to 4 fs. Spectral broadening induced by xenon generates content extending from 800 to 1200 nm, with a  $-10$  dB bandwidth of 430 nm. The d-scan RMS error is 2.1% and the measured compressed pulsewidth is 6.8 fs, corresponding to two optical cycles at a central wavelength of 1030 nm. The FTL pulsewidth is 5.9 fs and the temporal Strehl ratio is as high as 69%. The transmission of the capillary stage, including mode-matching optics and chirped mirrors, is 72%, and the overall transmission from the laser to the 2-optical cycle pulse is 61%. Taking into account the measured optical-to-optical efficiency of 46% for the laser source (including the grating compressor), the power amplifier pump diode-to-few cycle beam efficiency is 28%, probably the most efficient few-cycle source ever reported. As an example, similar efficiencies are estimated to be below 5% and 14% for state-of-the-art near-infrared OPCPA systems [6] or cascaded capillaries setups at 1030 nm [12]. As a result, the pulse energy at the output is 140  $\mu\text{J}$ , corresponding to an average power of 21 W.

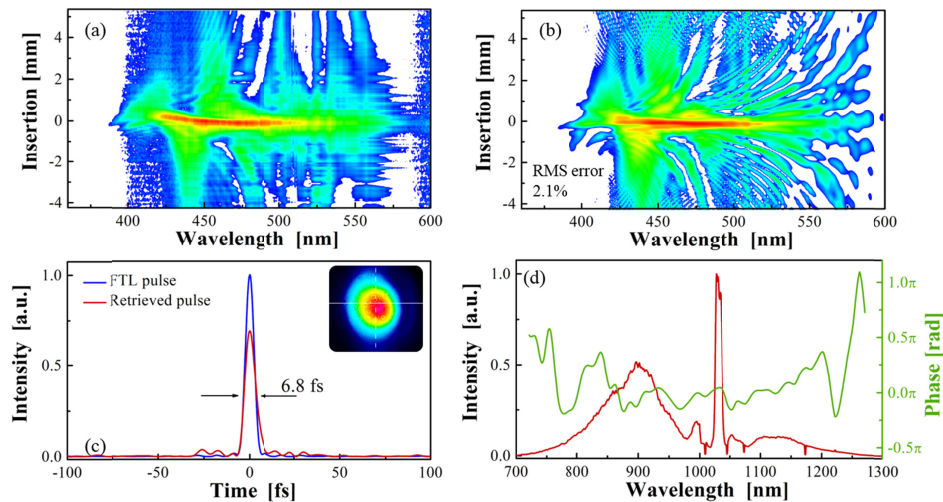


Fig. 5. Measured (a) and retrieved (b) d-scan traces at the output of the capillary stage. Temporal profile (c) (far-field spatial profile in inset) and spectral intensity and phase (d).

Spatial characterization of the compressed output is shown in Fig. 6. As expected at the output of a capillary, the mode profile is very clean, and the  $M^2$  factors are measured to be  $1.2 \times 1.2$ . Note that this measurement is made with a silicon-based camera and filters out the spectral content above 1.1  $\mu\text{m}$ . We also performed  $M^2$  measurement using an InGaAs CCD camera that reveals similar results.

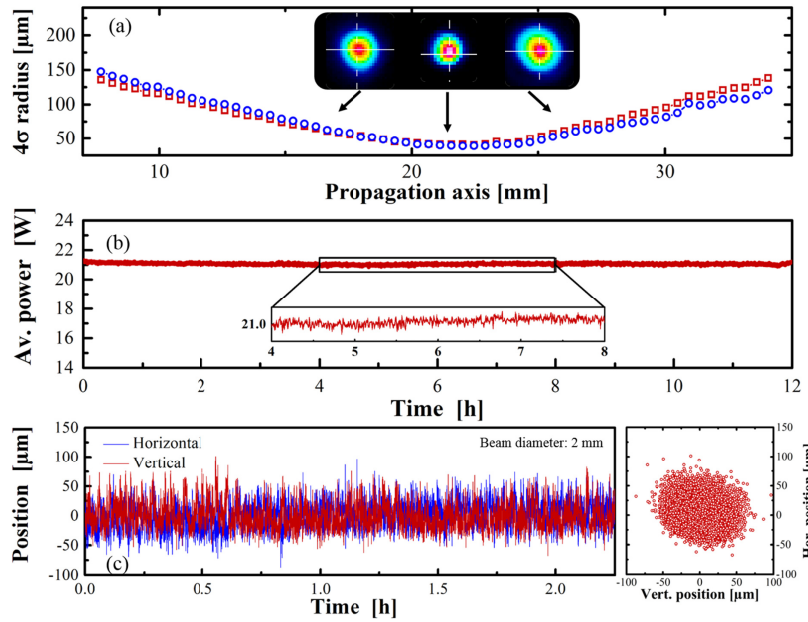


Fig. 6. Additional characterization at the output of the capillary. (a) Caustic measurement along two orthogonal axes. (b) Long-term power stability measurement at 21 W average power (inset: 0.5 W zoom around mean average power). (c) Beam pointing stability measurement.

At the output, stability properties are often an important aspect, in particular to drive highly nonlinear processes such as HHG. Thus, we characterize the output beam long term stability in terms of beam pointing and average power. These results are reported in Fig. 6. The RMS beam pointing deviation is 37  $\mu\text{m}$  over more than 2 hours, corresponding to beam deviations of less than 2% of the beam diameter. A long-term power stability of the few-cycle source is plotted in Fig. 6 over 12 hours with a mean average power of 21 W and a RMS deviation of 0.3%, showing that the source is undoubtedly well-suited to perform long runs of applications experiment.

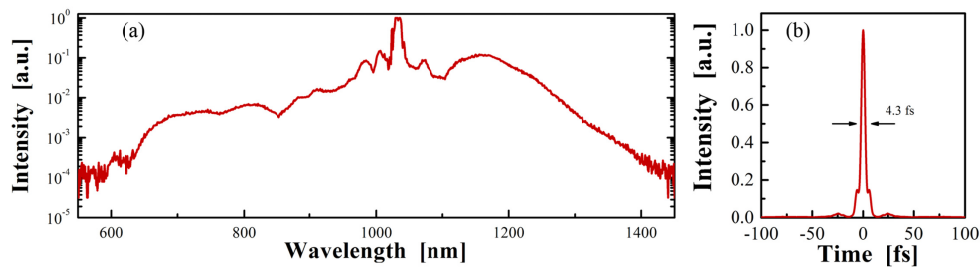


Fig. 7. (a) Broadest spectrum generated at the capillary output. (b) Corresponding Fourier transform limited temporal profile.

We also increase the xenon pressure to generate the broadest possible spectrum. We thus increase the pressure to 700 mbar, close to the critical pressure. At this pressure, the spectrum expands beyond the chirped mirrors reflectivity bandwidth and cannot be compressed. We measure the spectral profile by removing the compressor (see Fig. 7), showing a spectrum spanning more than 1 octave, from 600 nm to 1400 nm. The corresponding Fourier transform limit of this spectrum shows that sub-2 cycles pulses could be generated with such setup.



## 6. Relative intensity noise

We now focus on relative intensity noise (RIN) measurements along the system. For that purpose, RIN measurements are done using a fast photodiode and a low-pass filter with a cutoff frequency of 50 kHz to remove harmonics of the repetition rate (150 kHz). The signal is acquired using a digital oscilloscope and a fast Fourier transform is performed to obtain the RIN power spectral density.

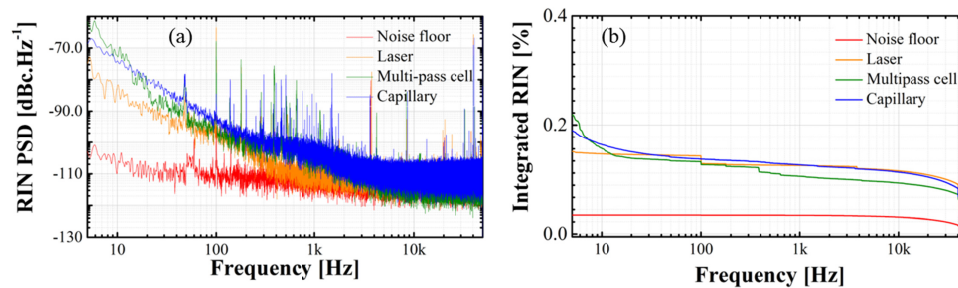


Fig. 8. Relative intensity noise power spectral density (a) and integrated RIN (b) measurement throughout the system.

The RIN power spectral densities measured at different points in the system are shown in Fig. 8 in the frequency range from 5 Hz to 50 kHz. At the output of the MPC, the total RMS RIN (integrated over 5 Hz to 50 kHz) is 0.21%, to be compared with 0.18% at the output of the laser. This shows propagation in the MPC does not bring additional noise contributions in this frequency range.

At the output of the capillary, the total RMS RIN (integrated over 5 Hz to 50 kHz) is 0.2%. Noise properties are thus dominated by the pump laser driving the nonlinear stages. These results also show the system's compatibility with CEP stabilization, where intensity noise properties are paramount to reduce amplitude-to-phase noise transfer mechanisms [25].

## 7. Conclusion

To summarize, we demonstrate a two-cycle-source based on a high-energy femtosecond YDFA followed by a hybrid two-stage nonlinear compression setup. The association of a MPC-based stage and large-diameter capillary stage provides a compression factor of 48 with an overall transmission of 61%. This source is, to the best of our knowledge, the most efficient few cycle high energy and high repetition rate laser demonstrated to date. It is very compact with an overall footprint of  $1.8 \text{ m} \times 1.0 \text{ m}$  and provides a stable train of few-cycle pulses at a central wavelength of 1030 nm over hours. The delivered 6.8 fs 140  $\mu\text{J}$  pulses at 150 kHz repetition rate (21 W average power) are ideally suited to drive high-photon flux XUV sources [26] through HHG. This architecture is also fully scalable since the use of both multipass cells and capillaries has been demonstrated at average power and energies beyond respectively 100 W [12,15] and 1 mJ [22]. We believe that future implementation of carrier-envelope phase stabilization on such laser systems will considerably expand the field of attosecond physics.

## Funding

Agence Nationale de la Recherche (ANR) (ANR-10-LABX-0039-PALM, ANR-16-CE30-0027-01); Conseil Départemental de l'Essonne (ASTRE Sophie).

## References

1. F. Lépine, M. Y. Ivanov, and M. J. J. Vrakking, "Attosecond molecular dynamics: fact or fiction?" *Nat. Photonics* **8**(3), 195–204 (2014).

2. F. Calegari, G. Sansone, S. Stagira, C. Vozzi, and M. Nisoli, "Advances in attosecond science," *J. Phys. B* **49**(6), 062001 (2016).
3. M. F. Ciappina, J. A. Pérez-Hernández, A. S. Landsman, W. A. Okell, S. Zharebtsov, B. Förg, J. Schötz, L. Seiffert, T. Fennel, T. Shaaran, T. Zimmermann, A. Chacón, R. Guichard, A. Zaïr, J. W. G. Tisch, J. P. Marangos, T. Witting, A. Braun, S. A. Maier, L. Roso, M. Krüger, P. Hommelhoff, M. F. Kling, F. Krausz, and M. Lewenstein, "Attosecond physics at the nanoscale," *Rep. Prog. Phys.* **80**(5), 054401 (2017).
4. M. Nisoli, S. De Silvestri, O. Svelto, R. Szipöcs, K. Ferencz, C. Spielmann, S. Sartania, and F. Krausz, "Compression of high-energy laser pulses below 5 fs," *Opt. Lett.* **22**(8), 522–524 (1997).
5. H. Fattahi, H. G. Barros, M. Gorjan, T. Nubbemeyer, B. Alsaif, C. Y. Teisset, M. Schultze, S. Prinz, M. Haefner, M. Ueffing, A. Alismail, L. Vámos, A. Schwarz, O. Pronin, J. Brons, X. T. Geng, G. Arisholm, M. Ciappina, V. S. Yakovlev, D.-E. Kim, A. M. Azzeer, N. Karpowicz, D. Sutter, Z. Major, T. Metzger, and F. Krausz, "Third-generation femtosecond technology," *Optica* **1**(1), 45–63 (2014).
6. F. J. Furch, T. Witting, A. Giree, C. Luan, F. Schell, G. Arisholm, C. P. Schulz, and M. J. J. Vrakking, "CEP-stable few-cycle pulses with more than 190  $\mu$ J of energy at 100 kHz from a noncollinear optical parametric amplifier," *Opt. Lett.* **42**(13), 2495–2498 (2017).
7. T. Nubbemeyer, M. Kaumanns, M. Ueffing, M. Gorjan, A. Alismail, H. Fattahi, J. Brons, O. Pronin, H. G. Barros, Z. Major, T. Metzger, D. Sutter, and F. Krausz, "1 kW, 200 mJ picosecond thin-disk laser system," *Opt. Lett.* **42**(7), 1381–1384 (2017).
8. P. Russbuehdt, T. Mans, J. Weitenberg, H. D. Hoffmann, and R. Poprawe, "Compact diode-pumped 1.1 kW Yb:YAG Innoslab femtosecond amplifier," *Opt. Lett.* **35**(24), 4169–4171 (2010).
9. M. Müller, M. Kienel, A. Klenke, T. Gottschall, E. Shestae, M. Plötner, J. Limpert, and A. Tünnermann, "1 kW 1 mJ eight-channel ultrafast fiber laser," *Opt. Lett.* **41**(15), 3439–3442 (2016).
10. J. Boulet, Y. Zaouter, J. Limpert, S. Petit, Y. Mairesse, B. Fabre, J. Higuier, E. Mével, E. Constant, and E. Cormier, "High-order harmonic generation at a megahertz-level repetition rate directly driven by an ytterbium-doped-fiber chirped-pulse amplification system," *Opt. Lett.* **34**(9), 1489–1491 (2009).
11. S. Hädrich, M. Krebs, A. Hoffmann, A. Klenke, J. Rothhardt, J. Limpert, and A. Tünnermann, "Exploring new avenues in high repetition rate table-top coherent extreme ultraviolet sources," *Light Sci. Appl.* **4**(8), e320 (2015).
12. S. Hädrich, M. Kienel, M. Müller, A. Klenke, J. Rothhardt, R. Klas, T. Gottschall, T. Eidam, A. Drozdy, P. Jójárt, Z. Várallyay, E. Cormier, K. Osvay, A. Tünnermann, and J. Limpert, "Energetic sub-2-cycle laser with 216 W average power," *Opt. Lett.* **41**(18), 4332–4335 (2016).
13. Y.-G. Jeong, R. Piccoli, D. Ferachou, V. Cardin, M. Chini, S. Hädrich, J. Limpert, R. Morandotti, F. Légaré, B. E. Schmidt, and L. Razzari, "Direct compression of 170-fs 50-cycle pulses down to 1.5 cycles with 70% transmission," *Sci. Rep.* **8**(1), 11794 (2018).
14. L. Lavenue, M. Natile, F. Guichard, Y. Zaouter, M. Hanna, E. Mottay, and P. Georges, "High-energy few-cycle Yb-doped fiber amplifier source based on a single nonlinear compression stage," *Opt. Express* **25**(7), 7530–7537 (2017).
15. J. Schulte, T. Sartorius, J. Weitenberg, A. Vernaleken, and P. Russbuehdt, "Nonlinear pulse compression in a multi-pass cell," *Opt. Lett.* **41**(19), 4511–4514 (2016).
16. M. Hanna, X. Dêlen, L. Lavenue, F. Guichard, Y. Zaouter, F. Druon, and P. Georges, "Nonlinear temporal compression in multipass cells: theory," *J. Opt. Soc. Am. B* **34**(7), 1340–1347 (2017).
17. M. Seidel, G. Arisholm, J. Brons, V. Pervak, and O. Pronin, "All solid-state spectral broadening: an average and peak power scalable method for compression of ultrashort pulses," *Opt. Express* **24**(9), 9412–9428 (2016).
18. F. Lu, P. Xia, Y. Matsumoto, T. Kanai, N. Ishii, and J. Itatani, "Generation of sub-two-cycle CEP-stable optical pulses at 3.5  $\mu$ m from a KTA-based optical parametric amplifier with multiple-plate compression," *Opt. Lett.* **43**(11), 2720–2723 (2018).
19. J. E. Beetar, S. Gholam-Mirzaei, and M. Chini, "Spectral broadening and pulse compression of a 400  $\mu$ J, 20 W Yb:KGW laser using a multi-plate medium," *Appl. Phys. Lett.* **112**(5), 051102 (2018).
20. J. Weitenberg, A. Vernaleken, J. Schulte, A. Ozawa, T. Sartorius, V. Pervak, H.-D. Hoffmann, T. Udem, P. Russbuehdt, and T. W. Hänsch, "Multi-pass-cell-based nonlinear pulse compression to 115 fs at 7.5  $\mu$ J pulse energy and 300 W average power," *Opt. Express* **25**(17), 20502–20510 (2017).
21. L. Lavenue, M. Natile, F. Guichard, Y. Zaouter, X. Delen, M. Hanna, E. Mottay, and P. Georges, "Nonlinear pulse compression based on a gas-filled multipass cell," *Opt. Lett.* **43**(10), 2252–2255 (2018).
22. M. Ueffing, S. Reiger, M. Kaumanns, V. Pervak, M. Trubetskov, T. Nubbemeyer, and F. Krausz, "Nonlinear pulse compression in a gas-filled multipass cell," *Opt. Lett.* **43**(9), 2070–2073 (2018).
23. J. K. Wahlstrand, Y.-H. Cheng, and H. M. Milchberg, "High field optical nonlinearity and the Kramers-Kronig relations," *Phys. Rev. Lett.* **109**(11), 113904 (2012).
24. M. Miranda, C. L. Arnold, T. Fordell, F. Silva, B. Alonso, R. Weigand, A. L'Huillier, and H. Crespo, "Characterization of broadband few-cycle laser pulses with the d-scan technique," *Opt. Express* **20**(17), 18732–18743 (2012).
25. A. Baltuska, M. Uiberacker, E. Goulielmakis, R. Kienberger, V. S. Yakovlev, T. Udem, T. W. Hänsch, and F. Krausz, "Phase-controlled amplification of few-cycle laser pulses," *IEEE J. Sel. Top. Quantum Electron.* **9**(4), 972–989 (2003).

26. A. Inés Gonzalez, G. Jargot, P. Rigaud, L. Lavenu, F. Guichard, A. Comby, T. Auguste, O. Sublemontier, M. Bougeard, Y. Zaouter, P. Georges, M. Hanna, and T. Ruchon, "Spatio-spectral structures in high harmonic generation driven by tightly focused high repetition rate lasers," *J. Opt. Soc. Am. B* **35**(4), A6–A14 (2018).